

# Convergence Analyses for Fluid-Structure Interaction Simulation in a Thin Hyper-elastic Pipe

Q. Lu\*, E. Guleryuz\*, M. Vellakal\*, A. Taha\*, S. Koric\*,\*\* and P. Cordoba\*\*\*

Corresponding author: qiyuelu1@illinois.edu

\* National Center for Supercomputing Applications

\*\* Department of Mechanical Science and Engineering

University of Illinois at Urbana-Champaign

Urbana, IL, U.S.A, 61801

\*\*\* Department of Computer Applications in Science and Engineering

Barcelona Supercomputing Center

Barcelona, Spain, 08034

**Abstract:** One of the difficulties in Fluid-Structure Interaction(FSI) co-simulations is the convergence within each time step, which include the convergence of each participating solver and the data transfer among them. Especially, when the solid material non-linearity or thin geometries are involved, there are typically large deformations which could eventually result in convergence difficulty and even the failure of numerical algorithms. Adopting a hyper-elastic pipe benchmark case, this paper explores the effects of different scale factors on the overall convergence in each co-simulation time step. Three constituent components are involved and dedicated to structure, fluid and system coupling, respectively. The coupling scheme is in two-way.

*Keywords:* Fluid-Structure Interaction, Convergence, Material Non-linearity, Numerical Algorithms

## 1 Introduction

FSI problems play prominent roles in many engineering fields, however, studies of these problems are still challenging due to the typical geometry and material non-linearities involved. The numerical method used to solve FSI problems can be generally fit into two categories: the monolithic approach and the partitioned approach. Representative numerical procedures in these two categories are reviewed and tested in the literatures including [1], [2], [3] and [4]. The two-way coupling scheme used in this paper is classified as the second approach, and *two-way* means that there are displacement data transferred from structure to fluid and force data transferred from fluid to structure. One challenging issue in FSI study is the stabilization and convergence of the numerical model, due to complicated physics involved. Unstable or hard-to-converge cases typically have one or more of these following features:

Thin structure for the solid part such as a shell or membrane;

Structural materials with a low Young's Modulus, E.g. hyper-elastic materials;

Gases or liquids modeled with constant density(incompressible, i.e. infinite speed of propagation of pressure perturbations).

Thin hyper-elastic structure brings geometry and material non-linearity into the model. These strongly coupled FSI cases are widely encountered in real-world engineering problems, such as in bioengineering

Name	Value	Units
Start Time	0	sec
End Time	1.6	sec
Time Step in System Coupling	0.0005	sec
<b>Mechanical</b>		
Number of substeps	1	
Solver Type	Direct	
Newton-Raphson Option	Unsymmetric	
Line Search	On	
Stabilization	Constant	
<b>Fluent</b>		
Model Type	Laminar	
Max Iterations/Time Step	20	
Scale factor(volume-based)	0/10/20/100	

Table 1: Parameters setup in ANSYS

fields[5]. Explorations on convergence issues in bio-mechanical applications such as arteries can be found in literature[6]. The flow regime in this paper is laminar, while turbulence model is also widely used for FSI simulation in certain circumstances, such as aortic blood flow, and relevant studies can be found in literature[7]. The solid part with above features are more sensitive to stress applied by fluids and prone to large deformation. This deformation causes the volume of fluid regime to vary and therefore affects the stress applied on the structure in return. In certain conditions, this can form a positive feedback mechanism and the oscillation with increasing magnitude will break the co-simulation in the first few iterations or time steps. On the other hand, incompressible approximation of fluid flow is usually known to be problematic in modeling the propagation of any disturbance in it, as predicting a speed equal to infinity for the propagation of the disturbance. The case studied in this paper includes all three features above and the participating solvers and modules are ANSYS Mechanical, Fluent and System Coupling. This paper illustrates that with other appropriate settings, different scale factors which correspond to series of preconditioning matrix have significant effects on the stabilization and convergence. The remaining part of this paper is arranged as follows: Section two is dedicated to the case setup. Section three focuses on simulations with different parameter settings and also results are presented there. Section four includes the verification. Conclusions and future work are discussed in section five.

## 2 Problem Statement

### 2.1 Case Setup

The case used in this article is a hyper-elastic pipe with fluid flowing through. The pipe wall is Mooney-Rivlin material(rubber) and its two-parameter model is used. Time-dependent pressures are applied on both inlet and outlet and their difference is the driving force for the fluid flow. This time-dependent Boundary Conditions(BCs) are realized by User Defined Functions(UDF). This benchmark case was first calculated and presented in literature[8]. The schematic of this case is shown in Figure 1. In this case, the coupling scheme is two-way, i.e. there are data being transferred bidirectionally between structure and fluid. Material properties and BCs are illustrated in Figure 1. Certain parameters in case setups are listed in Table 1, and default values are used for unlisted parameters. It is necessary to emphasize that, without scaling, i.e. when the value of scale factor is zero, this case is not stable initially. As shown in Figure 2, the integral of pressure on the pipe inner wall oscillates violently in first few implicit mesh update circles and the simulation aborts as expected. Therefore, in next section, the general principle behind this scale factor is discussed.

## 2.2 Mathematics Behind the Scale Factor

Generally following the literature [9], [10] and [11], mathematics behind scale factors are discussed here. The unsteady conservation equation for transport of a scalar quantity  $\Phi$  can be written in integral and conservative form for an arbitrary control volume  $V$  as follows

$$\frac{\partial}{\partial t} \int_V \rho \Phi dV + \int_{\partial V} \rho \Phi \vec{u} \cdot d\vec{A} = \int_{\partial V} \Gamma \nabla \Phi \cdot d\vec{A} + \int_V S_\Phi dV \quad (1)$$

With respect to dynamic meshes, this integral form on an arbitrary control volume,  $V$ , whose boundary is moving can be written as

$$\frac{\partial}{\partial t} \int_V \rho \Phi dV + \int_{\partial V} \rho \Phi (\vec{u} - \vec{u}_g) \cdot d\vec{A} = \int_{\partial V} \Gamma \nabla \Phi \cdot d\vec{A} + \int_V S_\Phi dV \quad (2)$$

where

$\rho$  = fluid density

$\vec{u}$  = flow velocity vector

$\vec{u}_g$  = mesh velocity of the moving mesh

$\Gamma$  = diffusion coefficient

$S_\Phi$  = source term of  $\Phi$

Here,  $\partial V$  is the boundary of the control volume  $V$ . This equation reveals how the displacement or velocity of the moving mesh applied on the governing equations of fluid flow. It is applied to each control volume, or cell, in the computational domain. Discretization of Equation 2 on a given cell can be expressed as

$$\frac{\partial \rho \Phi}{\partial t} V + \sum_f^{N_{faces}} \rho_f \Phi_f (\vec{u}_f - \vec{u}_{g,f}) \cdot \vec{A}_f = \sum_f^{N_{faces}} \Gamma_\phi \nabla \Phi_f \cdot \vec{A}_f + S_\Phi V \quad (3)$$

where

$N_{faces}$  = number of faces enclosing cell

$\Phi_f$  = value of  $\Phi$  convected through face  $f$

$\rho_f (\vec{u}_f - \vec{u}_{g,f}) \cdot \vec{A}_f$  = mass flux through face  $f$

$\vec{A}_f$  = area of face  $f$ , in vector form

$\nabla \Phi_f$  = gradient of  $\Phi$  at face  $f$

$V$  = cell volume

The general form discretized Equation 3 applies readily to unstructured meshes composed of arbitrary cells and then being solved. It contains the unknown scalar variable  $\Phi$  at the cell center as well as the unknown values in surrounding neighbor cells. Therefore, this equation in general is nonlinear with respect to these variables. A linearized form can be written as

$$a_P \Phi = \sum_{nb} a_{nb} \Phi_{nb} + b \quad (4)$$

where the subscript  $nb$  means neighbor cells, and  $a_P$  and  $a_{nb}$  are the linearized coefficients for  $\Phi$  and  $\Phi_{nb}$ . Similar operations can be applied on each cell in the mesh, that results in a set of algebraic equations with a sparse coefficient matrix. This linear system can be written eventually as

$$Ax = b \quad (5)$$

For this case, this linear system is solved using Gauss-Seidel(G-S) linear equation solver in conjunction with an algebraic multigrid(AMG) method. Solving this linear system is directly related to the model's stability and convergence speed. The information on multigrid method can be found in refrence[12] and is not discussed here.

It is well known that the convergence of G-S method is efficient if matrix  $A$  is diagonally dominant[13], otherwise, the case might not converge quickly or even be stable. For cases with strong fluid-structure interaction, stabilization is achieved through a boundary source coefficient introduced in the continuity equation, designed to improve the diagonal dominance of the matrix system in the cells adjacent to dynamic mesh boundary zones. Mathematically, superpositions are applied to elements on the diagonal. Two methods for this boundary source coefficient are available: volume-based and coefficient-based and only the first one is used for this work. The volume-based method uses the cell volume  $V$  to re-scale the diagonal entry of the linear matrix system corresponding to the discretized continuity equation  $a_{ij}$  as  $a_{ij,s}$

$$a_{ij,s} = a_{ij} + KV \quad \text{if } i = j \quad \forall i, j \in \{1, 2, \dots, n\} \quad (6)$$

The second method directly re-scale the diagonal entry of the linear matrix system corresponding to the discretized continuity equation in this way

$$a_{ij,s} = a_{ij} + Ka_{ij} \quad \text{if } i = j \quad \forall i, j \in \{1, 2, \dots, n\} \quad (7)$$

where  $K$  is the scale factor and  $n$  is the number of cells. Note that the value the user choose for  $K$  will only affect the rate of convergence, and will not affect the converged solution. This can be explained as follows: For a linear system shown in Equation 5, any superposition on its diagonal elements as in Equation 6, 7 is equivalent to left multiplying a nonsingular matrix  $P$  as

$$PAx = Pb \quad (8)$$

The elements of matrix  $P$  is determined by scale factor  $K$ , cell volume  $V$ , and  $a_{ij}$  which are all known.  $P$  is a preconditioner and the operation in Equation 8 therefore improves the diagonal dominance in this new linear system and thus numerical stability can be achieved. Apparently, the same unknowns are being solved or can be recovered so the stabilization has no effect on converged results. A higher scale factor results in more stabilization, however, the rate of convergence is not proportional to its value, especially when the system is over-damped. As it is illustrated in later sections, different scale factors have crucial effects on the system stabilization and the rate of convergence.

## 2.3 Dynamic Mesh Update Method

The update of dynamic mesh is essential to the co-simulation and the method of mesh updating used in this case is reviewed here by following the literature[11]. The displacement or velocity of the moving mesh on the interface are exposed to the solid deformation first. In this case, spring-based smoothing method is used to propagate the movement from interface to far-side. Smoothing is one of the dynamic mesh update methods provided. Compared to other methods like remeshing, when smoothing is used to adjust the mesh of a zone with a moving and/or deforming boundary, the interior nodes of the mesh move, but the number of nodes and their connectivity does not change. In this way, the interior nodes absorb the movement of the boundary.

For spring-based smoothing, the edges between any two mesh nodes are idealized as a network of interconnected springs. The initial spacings of the edges before any boundary motion constitute the equilibrium state of the mesh. A displacement at a given boundary node will generate a force proportional to the displacement along all the springs connected to the node. Using Hook's Law, the force on a mesh node can be written as

$$\vec{F}_i = \sum_j^{n_i} k_{ij}(\Delta \vec{x}_j - \Delta \vec{x}_i) \quad (9)$$

where  $\Delta \vec{x}_i$  and  $\Delta \vec{x}_j$  are the displacements of node  $i$  and its neighbor  $j$ ,  $n_i$  is the number of neighboring nodes connected to node  $i$ , and  $k_{ij}$  is the spring constant (or stiffness) between node  $i$  and its neighbor  $j$ .

The spring constant for the edge connecting nodes  $i$  and  $j$  is defined as

$$k_{ij} = \frac{k_{fac}}{\sqrt{|\vec{x}_i - \vec{x}_j|}} \quad (10)$$

where  $k_{fac}$  is the value of spring constant factor which the user can specify. In this case, the value 0 is used for this factor. That assures the interior nodes are not allowed to extend beyond the boundary.

At equilibrium, the net force on a node due to all the springs connected to the node must be zero. This condition results in an iterative equation such that

$$\Delta \vec{x}_i^{m+1} = \frac{\sum_j^{n_i} k_{ij} \Delta \vec{x}_j^m}{\sum_j^{n_i} k_{ij}} \quad (11)$$

where  $m$  is the iteration number.

Since displacements are known at the boundaries (after boundary node positions have been updated), Equation 11 is solved using a Jacobi iterative algorithm sweep on all interior nodes. At convergence, the positions can be updated such that

$$\vec{x}_i^{n+1} = \vec{x}_i^n + \Delta \vec{x}_i^{converged} \quad (12)$$

where  $n + 1$  and  $n$  are representing the next time step and the current time step, respectively.

## 2.4 Time Derivative

First order implicit formulation is used for the time discretization. A generic expression for this algorithm can be illustrated as:

$$\frac{\partial \Phi}{\partial t} = F(\Phi) \quad (13)$$

Using backward differences, the above equation is given by

$$\frac{\Phi^{n+1} - \Phi^n}{\Delta t} = F(\Phi) \quad (14)$$

where

$\Phi$  = a scalar quantity

$n + 1$  = the next time level,  $t + \Delta t$

$n$  = the current time level,  $t$

$n - 1$  = the previous time level,  $t - \Delta t$

And the implicit method is featured with evaluating  $F(\Phi)$  at the future time level

$$\frac{\Phi^{n+1} - \Phi^n}{\Delta t} = F(\Phi^{n+1}) \quad (15)$$

e.g.

$$\Phi^{n+1} = \Phi^n + \Delta t F(\Phi^{n+1}) \quad (16)$$

## 3 Case Simulation

### 3.1 Scale Factor Setup

The choosing of appropriate values of scale factor is a process of *trial and error*. Only volume-based factor is tested in this work.

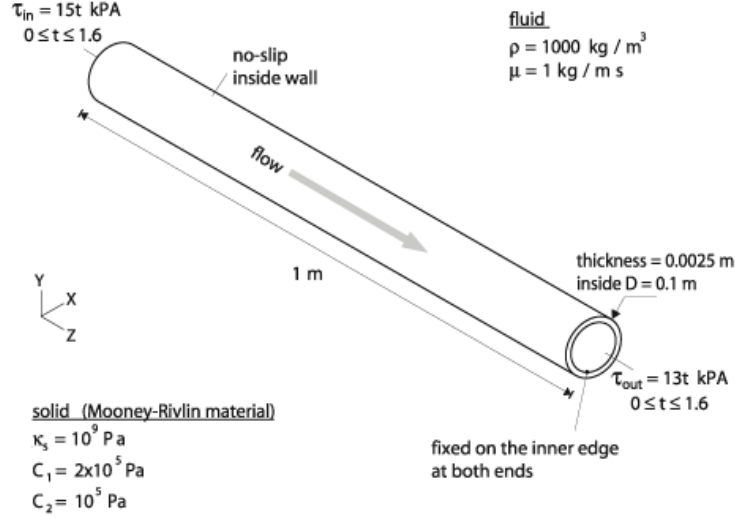


Figure 1: The schematic of the hyper-elastic pipe[8].  
 $\kappa_s$  is the bulk modulus.

In the first try, the volume-based scale factor is set as 10. Figure 3 illustrates the integral of pressure on fluid wall, however, the damping rate of oscillation is low and this case is not converged even after 40 implicit mesh updates. This is a clue that the value of scale factor doesn't provide enough scaling effects and larger numbers should be beneficial. Figure 3 covers the first time step only.

With volume-based scale factor set as 100, Figure 4 shows that the integral of pressure on fluid wall is very stable in the first system coupling time step. However, the plateau covers more than 400 iterations which is a sign that this curve is indeed over-damped, therefore the rate of convergence is impeded in the meanwhile. Figure 5 illustrates the continuity has a relatively low convergence slope while velocities reached convergence criteria in the first 7 implicit mesh updates. The whole simulation doesn't fully converge in the first time step until after 26 mesh updates, which corresponds to 520 iterations. Figure 4 and 5 cover the first time step only.

With scale factor set to 20, the system reaches convergence in the first 70 iterations, as shown in Figure 6. Additionally, the convergence of residuals and data transfer are considerably quick, as shown in Figure 7 and 8, compared to the over-damped scenario. Two time steps are covered in these figures. The following results are there presented with scale factor 20, unless exceptions are mentioned explicitly.

Another parameter which can affect the convergence is time step size. Changing the time step size for an already-well-converged system needs an appropriate changing in the scale factor in order to reach optimized convergence again. Time step size 0.0005 s is applied to most of data and graphs in this work. However, time step size 0.001 s is tested as well and the corresponding volume-based scale factor has to be 40 (instead of 20 while  $\Delta t = 0.0005 \text{ s}$ ) in order to get satisfactory rate of convergence. It is mentioned explicitly while  $\Delta t = 0.001 \text{ s}$  is used, otherwise,  $\Delta t = 0.0005 \text{ s}$  is applied. As time step size  $\Delta t$  in Equation 16 is one of denominators in discretization Equation 3, it eventually affects the coefficient matrix  $A$  in the linear system.

### 3.2 Case Simulation Results

With the volume-based scale factor set to 20, the simulation is run from 0 to 1.6 seconds physical time. Figure 9 illustrates the total mechanical strain of pipe wall at  $t = 1.6 \text{ s}$ . The maximum value is 0.391144 and the major contribution is on XY plane. The minimal value is 0.012494, and it represents the deformation of cells on the inlet and/or outlet.

Figure 10 shows the flow velocity contour at  $t = 1.6 \text{ s}$  on the mid-section plane. The maximum velocity is  $2.39926 \text{ m s}^{-1}$  which takes place at the position close to inlet. Because the no-slip boundary condition

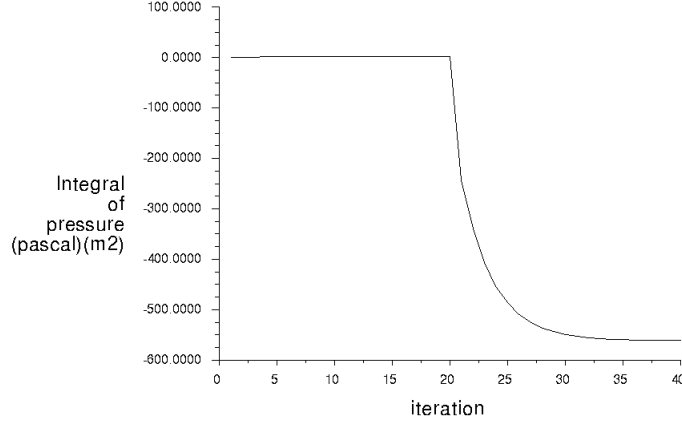


Figure 2: Integral of pressure diverges in first two mesh updates with volume-based scale factor = 0

is used on the inner wall of the pipe, therefore at each cross section perpendicular to  $Z$  axis, the velocity profile is approximately parabolic.

An interesting phenomenon is that there is reversed flow at the outlet until  $t = 0.513$  s around, therefore, before that time point, fluid is actually flowing into the pipe at both inlet and outlet and these fluids then occupy the expanded volume of the pipe. Figure 11 shows that at  $t = 0.4$  s, the velocity at the outlet is inward, pointing to the  $-Z$  direction. Figure 12 shows that at  $t = 0.6$  s, the velocity at the outlet at  $t = 0.6$  s switches to outward, pointing to the  $+Z$  direction. This can be verified in Figure 13 where mass flow rate at both inlet and outlet are recorded at each time step. Negative value there represents the flow at outlet is flowing into the pipe. Time step size 0.001 s (not the 0.0005 s in other plots) is applied to Figure 11, 12 and 13. They are revealing the same results as using time step size 0.0005 s.

## 4 Verification

This case is firstly benchmarked and presented in [8]. The maximum principal stretch there is 1.490, compared to the result in this paper: 1.391144. The minimal principal stretch in [8] is 1.081 while it is 1.012494 in this paper as reported in Section 3.2. Because the minimal stretch takes place on the cells at inlet and/or outlet, the finer meshes in this work account for this divergence on the minimal stretch value.

As mentioned previously, until  $t = 0.513$  s, the pipe is actually sucking fluid from both inlet and outlet, and this amount of incompressible fluid then fill up the swelled volume of the pipe. This statement can be verified this way: Based on Figure 13 and rectangular integration, the net mass of fluid which the pipe gained during  $t = [0, 1.6]$  s can be calculated and that is the area between these two curves. It is volume when this mass quantity is divided by fluid density and the volume equals to  $0.0067$   $m^3$ . On the other hand, the increased volume can be calculated by

$$(\pi D_i^2/4 - \pi D^2/4) \times L = 0.0073$$
  $m^3$  (17)

where  $D_i$  is the inflated pipe diameter using the maximum strain and  $D$  is the original pipe diameter. With the approximations assumed in this calculation, these two values can be considered matching.

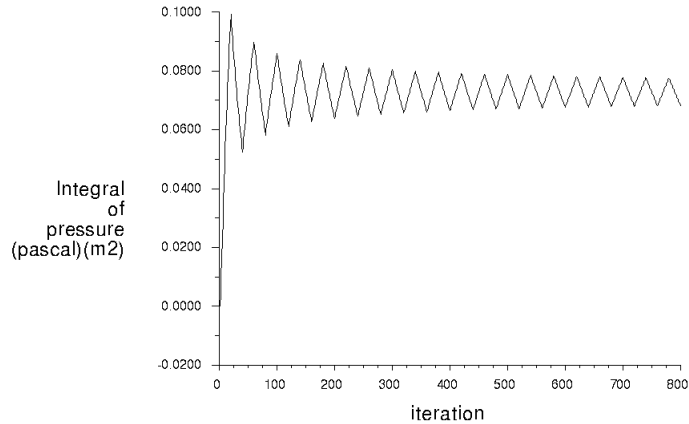


Figure 3: Integral of pressure ( $Pa \cdot m^2$ ) on fluid wall in the first system coupling step with volume-based scale factor = 10

## 5 Conclusion and Future Work

This paper investigates the effects of scale factors in the co-simulation of FSI by adopting a hyper-elastic thin pipe with fluid flowing through, for the objective of stabilizing the solving process. Results show that the appropriate scale factor not only can stabilize the solution, but also facilitate the problem’s rate of convergence. Different scale factors correspond to different preconditioning matrices on the linear system which arises after discretization and linearization. This resulting preconditioned system is therefore diagonally dominant which increases the stabilization of iterative solvers used in solving linear system and accelerates its rate of convergence. Time step size can affect the stabilization and rate of convergence, therefore, the chosen value of the scale factor for an optimized system is associated with specific time step size.

Future work may include the following items:

- discussing in more detail on the mathematics behind the scale factor, including space discretization techniques, preconditioners for Gauss-Siedel with AMG algorithm;
- analyzing the effect of different dynamic mesh update methods;
- conducting scalability analysis on the co-simulation approach on a High Performance Computer(HPC) platform;
- applying the experience in this paper on real-world engineering problems such as arteries, etc.;
- exploring turbulence model influence on the overall dynamics of FSI cases such as pulsatile flow in aortic simulation.

## References

- [1] G. Hou, J. Wang, and A. Layton. Numerical methods for fluid-structure interaction - a review. *Communications in Computational Physics*, 12:337–377, 2012.
- [2] Y. Bazilevs, K. Takizawa, and T. E. Tezduyar. *Computational Fluid-Structure Interactions: Methods and Applications*. Wiley, 2013.
- [3] B. Uekermann, J. C. Cajas, B. Gatzhammer, G. Houzeaux, M. Mehl, and M. Vázquez. Towards partitioned fluid-structure interaction on massively parallel systems. *Proceedings of WCCM XI/ECCM V/ECFD VI, Barcelona*, 2014.

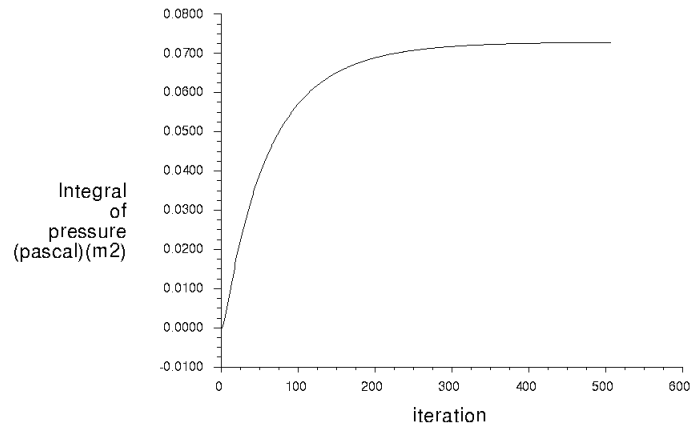


Figure 4: Integral of pressure ( $Pa \cdot m^2$ ) on fluid wall in the first system coupling step with volume-based scale factor = 100

- [4] S. Turek and J. Hron. Proposal for numerical benchmarking of fluid-structure interaction between an elastic object and laminar incompressible flow. *Fluid-Structure Interaction*, 53:371–385, 2006.
- [5] J. Hron and M. Madlik. Fluid-structure interaction with applications in biomechanics. *Nonlinear Analysis: Real World Applications*, 8:1431–1458, 2007.
- [6] L. Radtke, A. Larena-Avellaneda, E. S. Debus, and A. Duster. Convergence acceleration for partitioned simulations of the fluid-structure interaction in arteries. *Comput Mech*, 57:901–920, 2016.
- [7] K. M. Khanafer, J. L. Bull, and R. Berguer. Fluid-structure interaction of turbulent pulsatile flow within a flexible wall axisymmetric aortic aneurysm model. *European Journal of Mechanics - B/Fluids*, 28:88–102, 2009.
- [8] K. J. Bathe and G. A. Ledezma. Benchmark problems for incompressible fluid flows with structural interactions. *Computers & Structures*, 85:628–644, 2007.
- [9] J. Anderson. *Computational Fluid Dynamics*. McGraw-Hill Education, 1995.
- [10] P. K. Kundu, I. M. Cohen, and D. R. Dowling. *Fluid Mechanics*. Academic Press, 2012.
- [11] ANSYS Documentation. *Fluent Guide*. [Version 18.2], 2018.
- [12] W. L. Briggs, V. E. Henson, and S. F. McCormick. *A Multigrid Tutorial: Second Edition*. Society for Industrial and Applied Mathematics, 2000.
- [13] R. L. Burden and J. D. Faires. *Numerical Analysis*. Prindle, Weber & Schmidt, 1984.

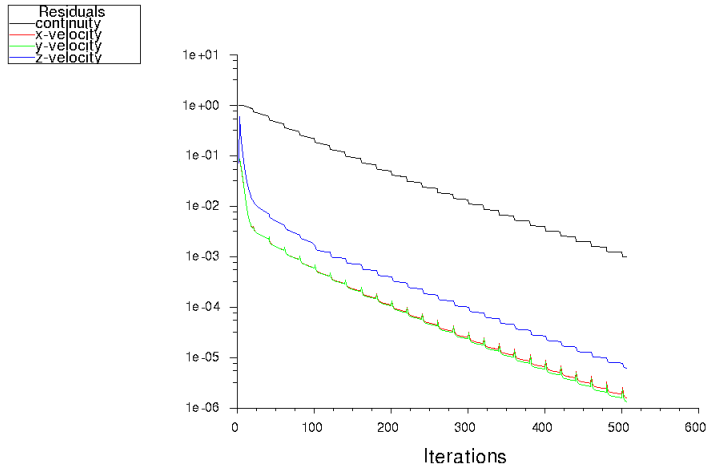


Figure 5: Residuals in the first system coupling step with volume-based scale factor = 100

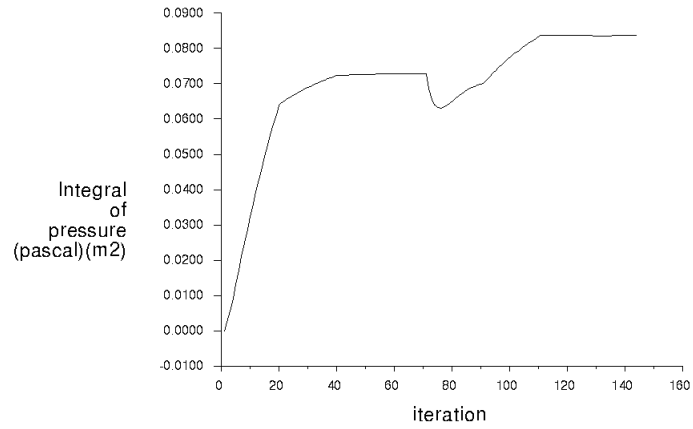


Figure 6: Integral of pressure in the first two system coupling steps with volume-based scale factor = 20

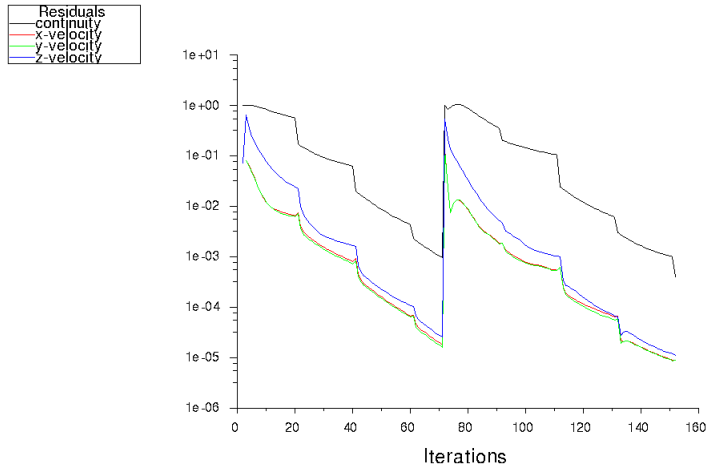


Figure 7: Residuals in the first two system coupling steps with volume-based scale factor = 20

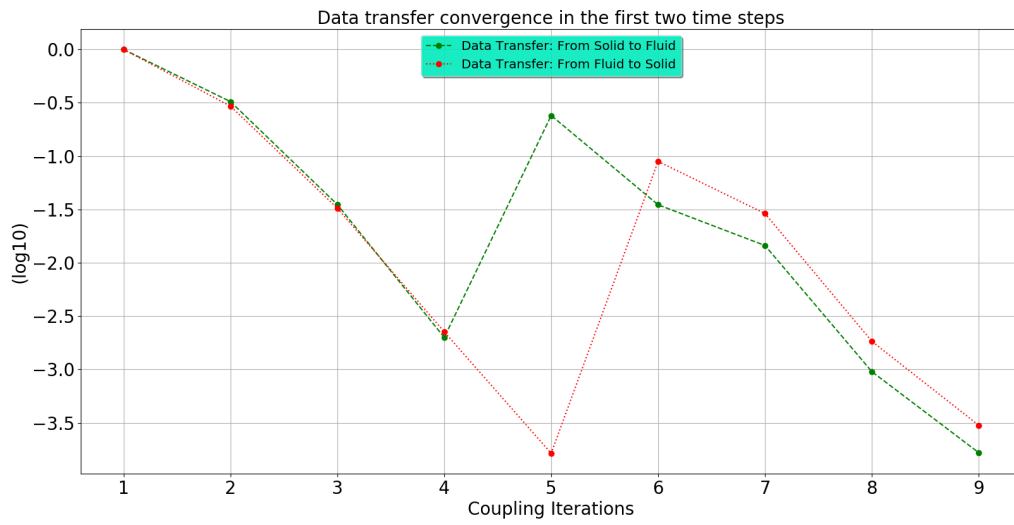


Figure 8: Data transfer in the first two system coupling steps with volume-based scale factor = 20

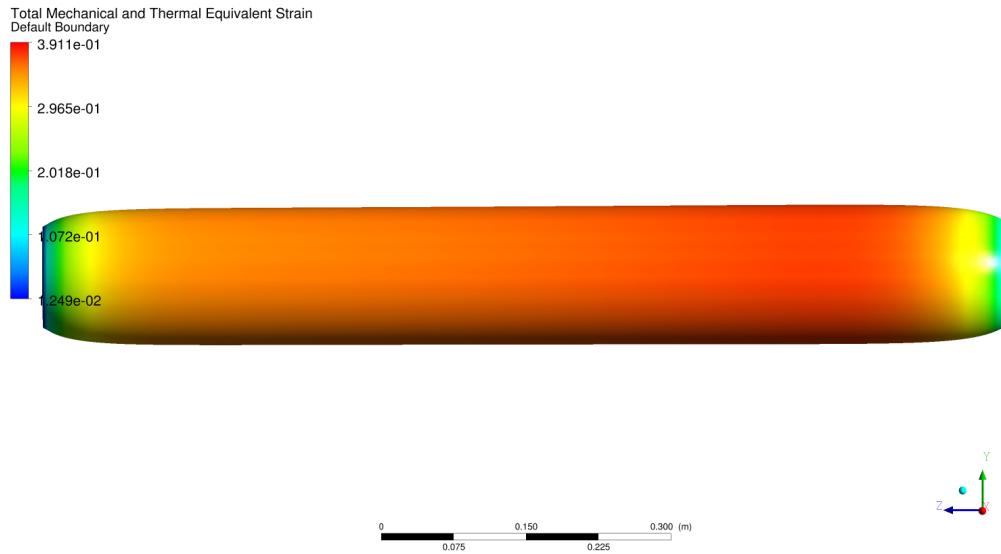


Figure 9: Total strain at  $t = 1.6s$  with volume-based scale factor = 20

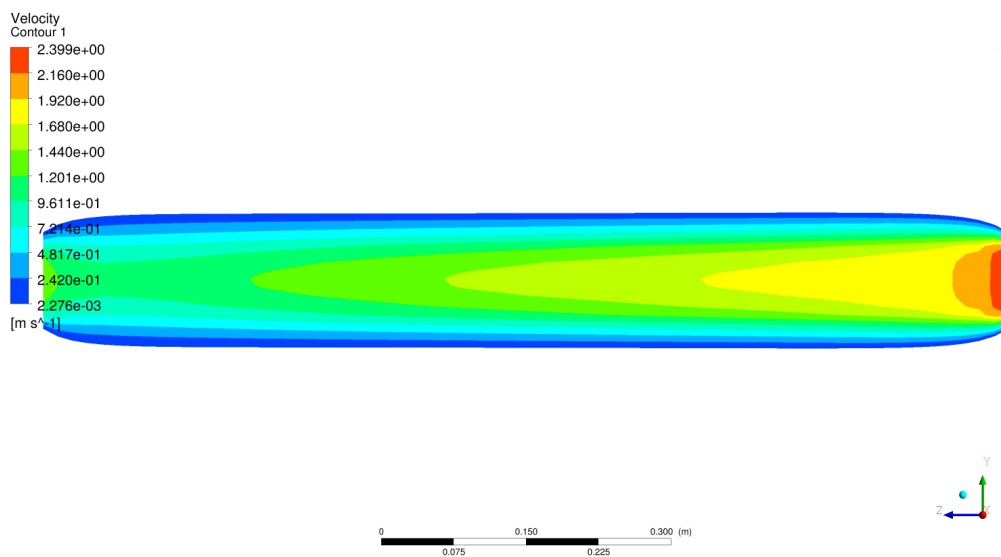


Figure 10: Flow velocity contour at  $t = 1.6s$  with volume-based scale factor = 20

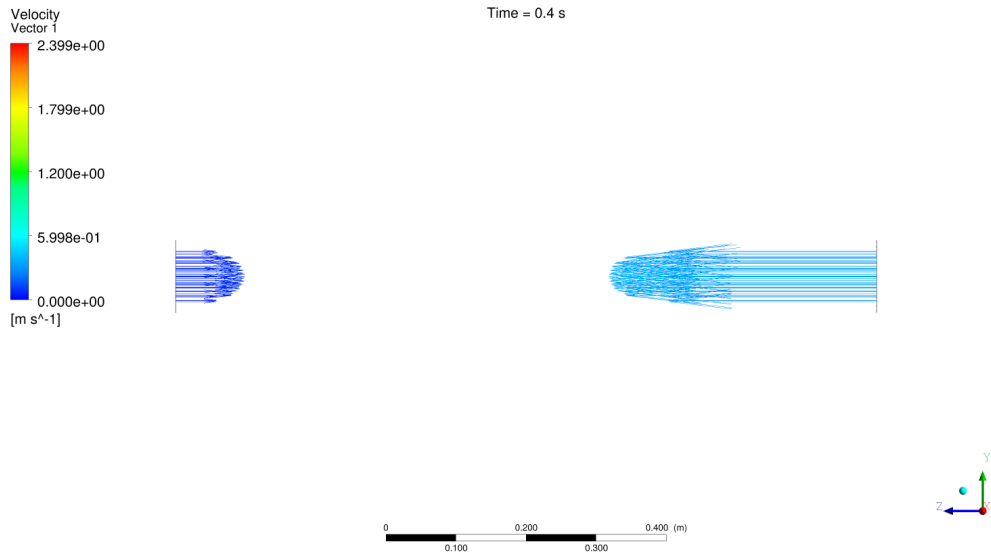


Figure 11: Flow velocity vector profile at both inlet and outlet with volume-based scale factor = 40, time step size = 0.001 s,  $t = 0.4$  s

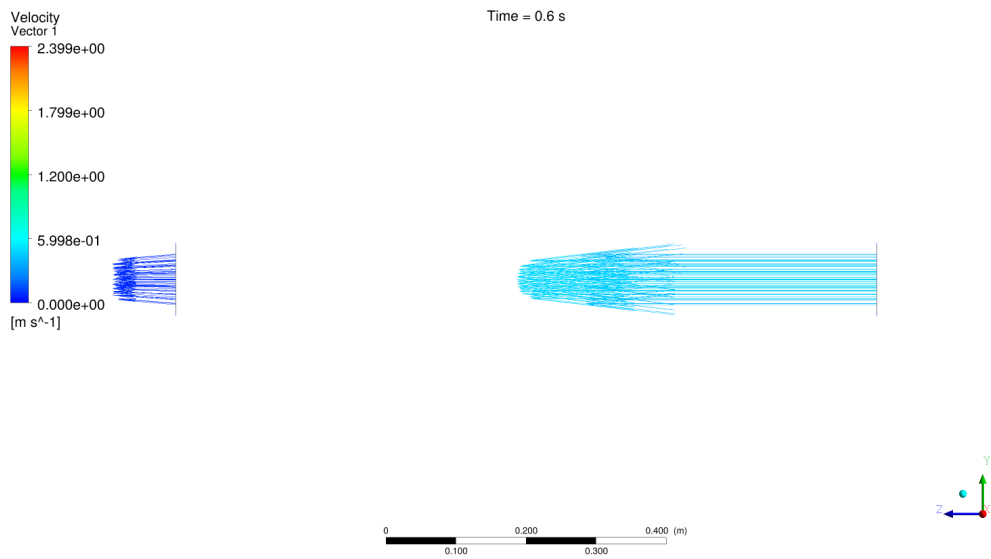


Figure 12: Flow velocity vector profile at both inlet and outlet with volume-based scale factor = 40, time step size = 0.001 s,  $t = 0.6$  s

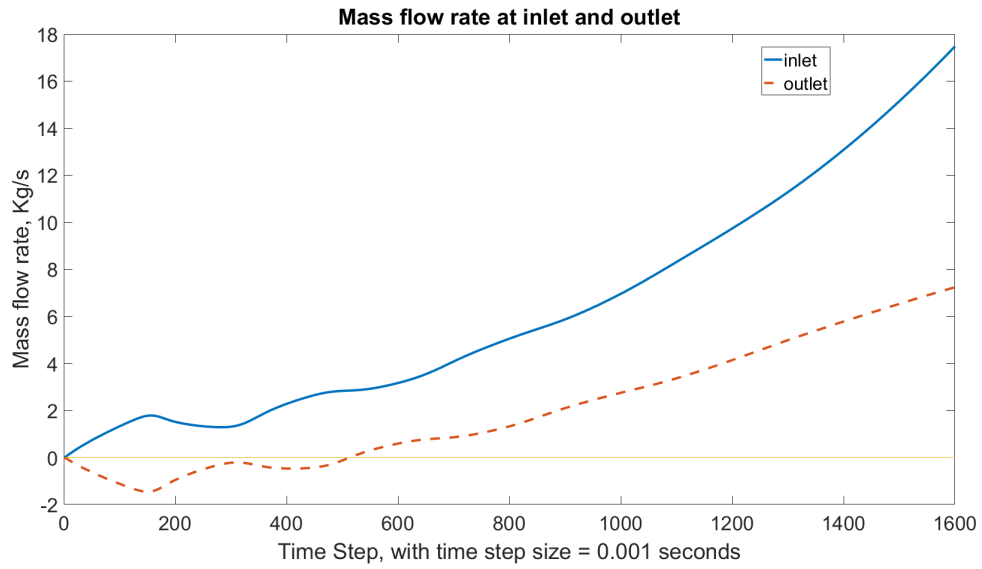


Figure 13: Mass flow rate at both inlet and outlet with volume-based scale factor = 40, time step size = 0.001 s